Nonlinear Analysis: Modelling and Control, Vol. 31, No. 6, 1319–1337
https://doi.org/10.15388/namc.2026.31.49070

Vilnius University Press

The Kuramoto–Tsuzuki equation: Invariant theory, bifurcation, chaotic behavior, and sensitivity analysis

Mir Sajjad Hashemi[a, 1], **Mushtaq K. Abdalrahem**[b,c], **Mohammad Esmael Samei**[d], **Kamyar Hosseini**[e,f,g], **Mustafa Bayram**[h]

[a] Department of Mathematics, University of Bonab, Bonab, Iran
hashemi_math396@yahoo.com

[b] College of Pharmacy, University of Al-Ameed, Iraq
Mushtaq.k@alameed.edu.iq

[c] Department of Statistics, College of Administration and Economics, University of Kerbala, Iraq

[d] Department of Mathematics, Faculty of Science, Bu-Ali Sina University, Hamedan, Iran
mesamei@basu.ac.ir; mesamei@gmail.com

[e] Department of Mathematics, Near East University, Mersin 10, Nicosia 99138, Turkey
kamyar_hosseini@yahoo.com

[f] Faculty of Engineering and Natural Sciences, Istanbul Okan University, Istanbul, Turkey

[g] Research Center of Applied Mathematics, Khazar University, Baku, Azerbaijan

[h] Computer Engineering, Biruni University, Istanbul, Turkey
mustafabayram@biruni.edu.tr

Received: April 2, 2026 / **Revised:** September 30, 2026 / **Published online:** October 15, 2026

Abstract. This paper investigates the Kuramoto–Tsuzuki equation through the application of the Lie symmetry method. We derive three Lie algebra generators pertinent to this equation, facilitating a transformation that reduces the partial differential equation to an ordinary differential equation. One of the reduced ordinary differential equations is solved analytically using Nucci's reduction method. The second reduced ordinary differential equation, derived from a combination of generators, is solved directly by some manipulations. Then we use a transformation to convert the Kuramoto–Tsuzuki equation into a second-order nonlinear ordinary differential equation. Utilizing a recently introduced technique, the second-degree generalized Abel equation method, we successfully obtain soliton solutions for the reduced ordinary differential equation. Additionally, we explore bifurcation phenomena and analyze phase portraits, providing deeper insights into the dynamic behavior of the system. The analysis of chaotic behavior and sensitivity of the corresponding

[1] Corresponding author.

© 2026 The Author(s). Published by Vilnius University Press
This is an Open Access article distributed under the terms of the Creative Commons Attribution Licence, which permits unrestricted use, distribution, and reproduction in any medium, provided the original author and source are credited.

dynamical system contributes to a better understanding of the Kuramoto–Tsuzuki equation and highlights the effectiveness of the proposed methods for analyzing complex nonlinear equations.

Keywords: Kuramoto–Tsuzuki equation, Lie symmetry method, generalized Abel equation method, dynamical behavior.

1 Introduction

Partial differential equation (PDEs) in complex domains play a central role in modeling and analyzing physical, biological, and engineering systems where geometry and boundary conditions are intricate. Unlike PDEs in simple domains, problems on irregular or multiconnected regions often arise in fluid dynamics, electromagnetics, material science, and medical imaging. Studying PDEs in these complex domains allows researchers to capture realistic behaviors such as wave propagation in heterogeneous media, stress distribution in composite structures, or heat transfer in irregular geometries. Advances in both analytical techniques and numerical methods for PDEs on complex domains are therefore crucial for bridging mathematical theory with real-world applications.

Solving complex PDEs requires a range of analytical and numerical approaches, each tailored to handle the nonlinearities and intricate boundary conditions often encountered [5, 8, 25]. Among these, the Lie symmetry method is particularly powerful, as it exploits the underlying symmetries of a PDE to reduce its order or transform it into a more tractable form, sometimes even yielding exact solutions. This method not only provides insights into invariant structures of the equations but also serves as a bridge between theory and computation. Beyond solution techniques, the study of bifurcation analysis is essential for understanding qualitative changes in system behavior when parameters vary, revealing transitions such as pattern formation or stability loss. Furthermore, many nonlinear PDEs exhibit chaotic dynamics where small perturbations in initial conditions can lead to drastically different outcomes. Identifying and analyzing such behavior is critical in fields ranging from fluid turbulence and climate modeling to biological systems, ensuring that models capture both predictable and unpredictable aspects of complex phenomena.

It seems that Kuramoto and Tsuzuki first established the equation known as the Kuramoto–Tsuzuki equation (KTE) for describing the dynamics of two-component systems near a bifurcation point in 1975 [17]. Since then, the equation has been extensively studied in various branches of applied mathematics and physics. One of the main applications of this equation is the modeling of various phenomena, including second-order phase transitions and nonlinear wave behavior. A remarkable one-dimensional case of the 2D Ginzburg–Landau equation is the 1D KTE [6,18,28]. In general, the KTE is formulated by

$$\frac{\partial u(\mathbf{x},t)}{\partial t} = (1+\mathrm{i}c_1)\Delta u(\mathbf{x},t) + \gamma u(\mathbf{x},t) - (1+\mathrm{i}c_2)\big|u(\mathbf{x},t)\big|^2 u(\mathbf{x},t) \tag{1}$$

for $\mathbf{x} \in \mathbb{R}^d$, $d = 1, 2, 3$, $t > 0$, where u is a complex-valued function, i is the imaginary unit, $c_1, c_2 \in \mathbb{R}$, and γ is a general parameter [30]. Stability of difference schemes for

solving the KTE and an a priori error estimate were investigated in [13]. In this paper, we consider Eq. (1) in one-dimensional case ($d = 1$).

Physically, in Eq. (1), $u(\mathbf{x}, t)$ represents the complex-valued, slowly varying amplitude of an oscillatory mode whose homogeneous steady state has just lost stability at a Hopf bifurcation point. The parameter γ measures the distance from the bifurcation threshold (the linear growth rate of the unstable mode); the term $(1 + \mathrm{i}c_1)\Delta u$ describes diffusive coupling together with a linear frequency-dispersion correction proportional to c_1; and the cubic term $(1 + \mathrm{i}c_2)|u|^2 u$ describes nonlinear saturation of the growing mode together with an amplitude-dependent nonlinear frequency correction proportional to c_2.

In this sense, the KTE is not a fundamental equation tied to a specific medium but a universal *amplitude* (or *envelope*) equation, structurally identical to the complex Ginzburg–Landau equation [1,10,24], and it governs the leading-order dynamics of essentially any spatially extended dissipative system near the onset of an oscillatory (Hopf) instability, independent of microscopic detail. Equations of this class describe, qualitatively and often quantitatively, a broad range of phenomena including nonlinear waves, second-order phase transitions, and pattern formation, with applications spanning superconductivity, superfluidity, Bose–Einstein condensation, nonlinear optics, hydrodynamics, and plasmas [1, 9].

Prior work on the KTE has proceeded largely along two separate lines. On the numerical side, various schemes have been developed and analyzed for stability and convergence, including Crank–Nicolson Galerkin finite element methods [28], split-step pseudospectral schemes [6], finite difference approaches [18], and linearly compact difference schemes for the two-dimensional case [30], alongside a priori error and convergence analyses of difference schemes for the equation [13]. On the analytical side, Lie symmetry methods, bifurcation theory, and soliton-construction techniques have been applied extensively to related nonlinear wave and Schrödinger-type models [7, 15, 16], but their systematic joint application to the KTE—including a full symmetry classification, closed-form soliton families, and an accompanying bifurcation/chaos analysis of the reduced dynamical system—has remained comparatively unexplored. The present work addresses this gap by combining Lie symmetry reduction, Nucci's reduction technique, and the second-degree generalized Abel equation method (GAEM) to construct new exact soliton solutions of the KTE, and by complementing these exact solutions with a bifurcation, chaotic behavior, and sensitivity analysis of the associated planar dynamical system.

This study was driven by two main concerns. First, although the KTE is already well established for modeling oscillator systems near bifurcation, a full Lie symmetry classification of this equation using modern solution methods such as the second-degree GAEM has not yet been reported. Second, finding exact solutions is only half the story, as it tells us nothing about whether those solutions actually hold up under real-world conditions. We also need to understand their stability, sensitivity to initial conditions, and how chaos might emerge. By tackling both issues together (finding new solutions and considering dynamical behavior), we give this study its real purpose and direction.

The paper is organized as follows. Section 2 presents the Lie symmetry method for KTE (1) and its symmetry reductions. Section 3 constructs soliton solutions using the second-degree GAEM. Section 4 is devoted to the study of bifurcation structures, the

analysis of chaotic behavior, and sensitivity analysis of the KTE. Finally, Section 5 summarizes the main results and contributions.

2 Lie symmetry method

One of the powerful analytical techniques used to study and solve complex PDEs by exploiting their underlying continuous symmetries is the Lie symmetry method, which was developed by Sophus Lie and systematically identifies transformation groups that leave a given PDE invariant, enabling the reduction of variables, simplification of equations, or direct construction of exact solutions. For complex PDEs such as those in nonlinear wave propagation, fluid dynamics, quantum mechanics, and mathematical physics, Lie symmetries provides insight into conserved quantities, invariant solutions, and integrability properties [7, 15, 16]. By revealing the geometric and algebraic structure of equations, the method offers a unifying framework that bridges analytical solution techniques and deeper theoretical understanding.

We aim to derive a system of KTEs equivalent to Eq. (1). To this end, we apply the following transformation:

$$u(x,t) = \Upsilon + \mathrm{i}\Phi \tag{2}$$

with the real-valued functions $\Upsilon = \Upsilon(x,t)$ and $\Phi = \Phi(\mathbf{x},t)$. By separating the real and imaginary components and setting each to zero, we obtain the coupled system of differential equations

$$\begin{aligned}
&\Upsilon_{xx} - c_1\Phi_{xx} - \Upsilon_t - \Upsilon^3 + c_2\Phi\Upsilon^2 + \big(-\Phi^2+\gamma\big)\Upsilon + c_2\Phi^3 = 0,\\
&c_1\Upsilon_{xx} + \Phi_{xx} - \Phi_t - \Phi^3 - c_2\Phi^2\Upsilon + \big(-\Upsilon^2+\gamma\big)\Phi - c_2\Upsilon^3 = 0.
\end{aligned}$$

This section describes the Lie symmetry method used to derive infinitesimals [4]. In this case, we examine one-parameter transformations as outlined below:

$$\begin{aligned}
t^* &= t + \epsilon\varpi_1 + O\big(\epsilon^2\big), \qquad & x^* &= x + \epsilon\varpi_2 + O\big(\epsilon^2\big),\\
\Upsilon^* &= \Upsilon + \epsilon\delta_1 + O\big(\epsilon^2\big), \qquad & \Phi^* &= \Phi + \epsilon\delta_2 + O\big(\epsilon^2\big)
\end{aligned} \tag{3}$$

in which $\varpi_i = \varpi_i(x,t,\Upsilon,\Phi)$, $\delta_i = \delta_i(x,t,\Upsilon,\Phi)$, $i = 1,2$, are infinitesimals with respect to $\mathfrak{X} = (x,t,\Upsilon,\Phi)$. In relation to the Lie transformations presented in (3), we derive the infinitesimal generators

$$\Gamma = \varpi_1\frac{\partial}{\partial t} + \varpi_2\frac{\partial}{\partial x} + \delta_1\frac{\partial}{\partial\Upsilon} + \delta_2\frac{\partial}{\partial\Phi}$$

and corresponding prolongation

$$\mathrm{Pr}^{(2)}\Gamma = \Gamma + \delta_1^x\frac{\partial}{\partial\Upsilon_x} + \delta_1^{xt}\frac{\partial}{\partial\Upsilon_{xt}} + \delta_1^{xx}\frac{\partial}{\partial\Upsilon_{xx}} + \cdots,$$

where δ_1^x, δ_1^{xx}, δ_1^{xt}, δ_2^x, δ_2^{xt}, and δ_2^{xx} are prolonged infinitesimals. A collection of nonlinear PDEs is obtained by substituting the values of the prolonged infinitesimals and

then equating the coefficients of various derivative terms to zero. By solving this system, we arrive at

$$\varpi_1 = R_1, \quad \varpi_2 = R_2, \qquad \delta_1 = -R_3 c_1 \Phi, \quad \delta_2 = R_3 c_1 \Upsilon.$$

The corresponding solutions for the infinitesimal generators Γ_j are determined by the arbitrary constants R_j, $j = 1, 2, 3$, and can be expressed as

$$\Gamma_1 = \frac{\partial}{\partial t}, \qquad \Gamma_2 = \frac{\partial}{\partial x}, \qquad \Gamma_3 = -c_1 \Phi \frac{\partial}{\partial \Upsilon} + c_1 \Upsilon \frac{\partial}{\partial \Phi}.$$

2.1 Reduction by the generator $\Gamma_1 + c\Gamma_2$ of Lie algebra

In this case, the generator corresponds to the traveling wave solution of Eq. (1)

$$\Gamma_1 + c\Gamma_2 = \frac{\partial}{\partial t} + c\frac{\partial}{\partial x}.$$

The similarity variables associated with this generator can be represented as

$$\Upsilon(x,t) = \mathcal{Z}_1(\xi), \quad \Phi(x,t) = \mathcal{Z}_2(\xi), \quad \xi = x - ct,$$

where $\mathcal{Z}_1(\xi)$ and $\mathcal{Z}_2(\xi)$ are solutions to the following system of ordinary differential equations (ODEs):

$$\begin{aligned}
&-\mathcal{Z}_1^3 + c_2 \mathcal{Z}_2 \mathcal{Z}_1^2 + \left(-\mathcal{Z}_2^2 + \gamma\right)\mathcal{Z}_1 + c_2 \mathcal{Z}_2^3 \\
&\quad + c\left(\frac{\mathrm{d}}{\mathrm{d}\xi}\mathcal{Z}_1\right) - c_1\left(\frac{\mathrm{d}^2}{\mathrm{d}\xi^2}\mathcal{Z}_2\right) + \frac{\mathrm{d}^2}{\mathrm{d}\xi^2}\mathcal{Z}_1 = 0, \\
&-\mathcal{Z}_2^3 - c_2 \mathcal{Z}_2^2 \mathcal{Z}_1 + \left(-\mathcal{Z}_1^2 + \gamma\right)\mathcal{Z}_2 - c_2 \mathcal{Z}_1^3 \\
&\quad + c\left(\frac{\mathrm{d}}{\mathrm{d}\xi}\mathcal{Z}_2\right) + c_1\left(\frac{\mathrm{d}^2}{\mathrm{d}\xi^2}\mathcal{Z}_1\right) + \frac{\mathrm{d}^2}{\mathrm{d}\xi^2}\mathcal{Z}_2 = 0.
\end{aligned}$$

By assuming $\mathcal{Z}_1 = -\mathcal{Z}_2$, we obtain

$$2\mathcal{Z}_2^3 - c\left(\frac{\mathrm{d}}{\mathrm{d}\xi}\mathcal{Z}_2\right) - \gamma \mathcal{Z}_2 - \frac{\mathrm{d}^2}{\mathrm{d}\xi^2}\mathcal{Z}_2 = 0. \tag{4}$$

To solve Eq. (4), we employ Nucci's reduction method [2, 22, 23]. According to this reduction technique, we will assume a change of variables [29]

$$\varkappa_1(\xi) = \mathcal{Z}_2(\xi), \qquad \varkappa_2(\xi) = \mathcal{Z}_2'(\xi).$$

These assumptions lead to the following system of ODEs from Eq. (4):

$$\varkappa_1' = \varkappa_2, \qquad \varkappa_2' = 2\varkappa_1^2 - c\varkappa_2 - \gamma\varkappa_1. \tag{5}$$

Selecting $\varkappa_1$ as a new independent variable converts system (5) into

$$\frac{\mathrm{d}\varkappa_2(\varkappa_1)}{\mathrm{d}\varkappa_1} = \frac{2\varkappa_1^2 - c\varkappa_2(\varkappa_1) - \gamma\varkappa_1}{\varkappa_2(\varkappa_1)}. \tag{6}$$

Let us construct the solution of Eq. (6) as

$$\varkappa_2(\varkappa_1) = q_2\varkappa_1^2 + q_1\varkappa_1 + q_0, \tag{7}$$

where q_i, $i = 0, 1, 2$, are unknown constants to be determined. Substituting Eq. (7) into Eq. (6) concludes a fifth-order polynomial with respect to the variable $\varkappa_1$. Vanishing the coefficients of obtained polynomial gives the following algebraic system:

$$\begin{aligned}
&-q_0^2(c+q_1) = 0,\\
&-q_0(c+q_1)q_1 - \big(cq_1 + 2q_0q_2 + q_1^2 + \gamma\big)q_0 = 0,\\
&-q_0(c+q_1)q_2 - \big(cq_1 + 2q_0q_2 + q_1^2 + \gamma\big)q_1 - q_2(c+3q_1)q_0 = 0,\\
&-\big(cq_1 + 2q_0q_2 + q_1^2 + \gamma\big)q_2 - q_2(c+3q_1)q_1 - \big(2q_2^2 - 2\big)q_0 = 0,\\
&-q_2^2(c+3q_1) - \big(2q_2^2 - 2\big)q_1 = 0,\\
&-\big(2q_2^2 - 2\big)q_2 = 0.
\end{aligned}$$

Solving this system implies the following solutions: $q_0 = 0$, $q_1 = -c/3$, $q_2 = \pm 1$, and $\gamma = 2c^2/9$. Therefore,

$$\varkappa_2^{\pm}(\varkappa_1) = \pm\varkappa_1^2 - \frac{1}{3}c\varkappa_1.$$

Now, if we return $\varkappa_1$ as the dependent variable, from the first equation of Eq. (5) we have

$$\varkappa_1'(\xi) = \pm\varkappa_1^2(\xi) - \frac{1}{3}c\varkappa_1(\xi). \tag{8}$$

Directly solving Eq. (8), we obtain

$$\varkappa_1(\xi) = c\left[\pm 3 + C_1 c\left(\sinh\frac{c\xi}{3} + \cosh\frac{c\xi}{3}\right)\right]^{-1}.$$

Hence,

$$\begin{aligned}
\mathcal{Z}_2^{\pm}(\xi) &= c\left[\pm 3 + C_1 c\left(\sinh\frac{c\xi}{3} + \cosh\frac{c\xi}{3}\right)\right]^{-1},\\
\mathcal{Z}_1^{\pm}(\xi) &= c\left[\mp 3 - C_1 c\left(\sinh\frac{c\xi}{3} + \cosh\frac{c\xi}{3}\right)\right]^{-1}.
\end{aligned}$$

Thus, from Eq. (2) we have

$$u^{\pm}(x,t) = (-1+\mathrm{i})c\left[C_1 c\left[\cosh\frac{c(ct-x)}{3} - \sinh\frac{c(ct-x)}{3}\right] \pm 3\right]^{-1}. \tag{9}$$

Figure 1 shows kink soliton $|u^+(x,t)|^2$ and singular solution $|u^-(x,t)|^2$ with respect to the parameters $C_1 = -1$ and $c = 2$ reported in Eq. (9).

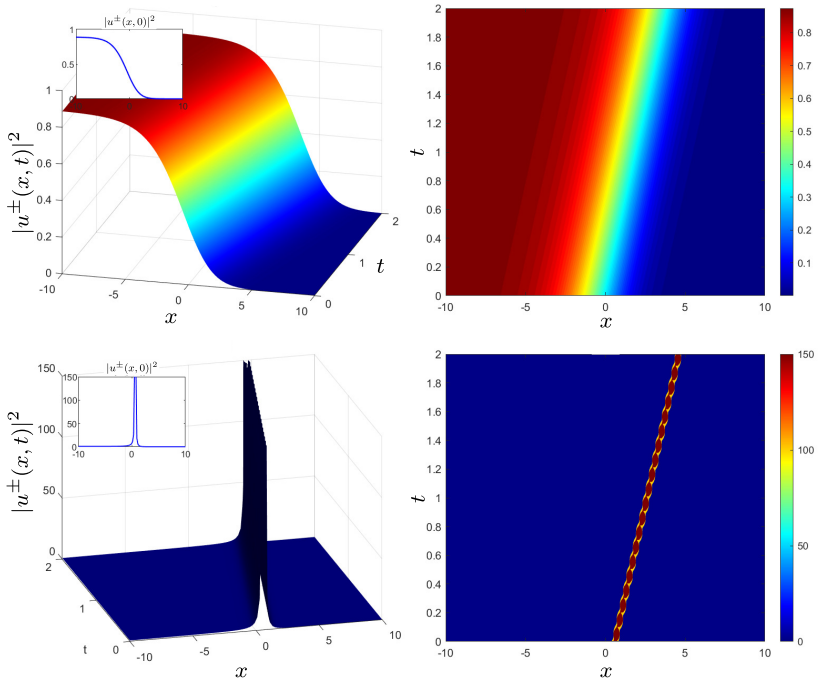


Figure 1. 3D plots and contour plots of $|u^{\pm}(x,t)|^2$ in Eq. (9).

2.2 Reduction by the generator $\Gamma_2 + \Gamma_3/c_1$ of Lie algebra

In this case, we have

$$\Gamma_2 + \frac{1}{c_1}\Gamma_3 = \frac{\partial}{\partial x} - \Phi\frac{\partial}{\partial \Upsilon} + \Upsilon\frac{\partial}{\partial \Phi}.$$

The similarity variables associated with this generator can be represented as

$$\begin{aligned} \Upsilon(x,t) &= \mathcal{Z}_1(\xi)\sin x + \mathcal{Z}_2(\xi)\cos x, \\ \Phi(x,t) &= -\mathcal{Z}_1(\xi)\cos x + \mathcal{Z}_2(\xi)\sin x. \end{aligned} \tag{10}$$

Here $\xi = t$, $\mathcal{Z}_1(\xi)$, and $\mathcal{Z}_2(\xi)$ are solutions to the following system:

$$\begin{aligned} &\frac{\mathrm{d}}{\mathrm{d}\xi}\mathcal{Z}_1 + \mathcal{Z}_1^3 - c_2\mathcal{Z}_1^2\mathcal{Z}_2 + \mathcal{Z}_2^2\mathcal{Z}_1 - \gamma\mathcal{Z}_1 + \mathcal{Z}_1 - c_2\mathcal{Z}_2^3 - c_1\mathcal{Z}_2 = 0, \\ &-\frac{\mathrm{d}}{\mathrm{d}\xi}\mathcal{Z}_2 - c_2\mathcal{Z}_1^3 - \mathcal{Z}_2\mathcal{Z}_1^2 - c_2\mathcal{Z}_1\mathcal{Z}_2^2 - c_1\mathcal{Z}_1 - \mathcal{Z}_2^3 + \gamma\mathcal{Z}_2 - \mathcal{Z}_2 = 0. \end{aligned} \tag{11}$$

By assuming $\mathcal{Z}_1(\xi) = \mathcal{Z}_2(\xi)$, we have $\mathrm{d}\mathcal{Z}_2/\mathrm{d}\xi) + 2\mathcal{Z}_2^3 + (1-\gamma)\mathcal{Z}_2 = 0$. By direct solving of this equation, we get

$$\mathcal{Z}_1(\xi) = \mathcal{Z}_2(\xi) = \frac{\sqrt{(C_1\gamma - C_1 + 2\,\mathrm{e}^{(2\gamma-2)\xi})\mathrm{e}^{(2\gamma-2)\xi}(\gamma-1)}}{C_1\gamma - C_1 + 2\,\mathrm{e}^{(2\gamma-2)\xi}}.$$

This solution satisfies system (11) by assuming $C_1 = 0$ and $c_1 = c_2(1-\gamma)$. Therefore,

$$\mathcal{Z}_1(\xi) = \mathcal{Z}_2(\xi) = \frac{\sqrt{2}}{2}\sqrt{\mathrm{e}^{4(\gamma-1)\xi}(\gamma-1)}\,\mathrm{e}^{-2(\gamma-1)\xi}.$$

Using Eq. (10), the solution of Eq. (1) is obtained as

$$u(x,t) = \frac{1+\mathrm{i}}{\sqrt{2}}\sqrt{\frac{(\mathrm{e}^{ct})^4(\mathrm{e}^{\gamma x})^4(\gamma-1)}{(\mathrm{e}^{c\gamma t})^4(\mathrm{e}^{x})^4}}\,\mathrm{e}^{2(\gamma-1)(ct-x)}.$$

3 Soliton solutions

In order to derive the soliton solution of model, let us consider the transformation

$$u(x,t) = V(\xi)\,\mathrm{e}^{\mathrm{i}\phi(x,t)}, \quad \xi = B_1 x - \nu t, \qquad \phi(x,t) = -k_1 x + wt + \theta, \tag{12}$$

where B_1 is the spatial scale of the envelope pattern, ν denotes the group velocity, k_1 is the wave number, w denotes the angular frequency, and θ is the initial phase.

By substituting Eq. (12) into Eq. (1), we obtain real and imaginary parts

$$V^3(\xi) + \left(k_1^2 - \gamma\right)V(\xi) - \left(\nu + 2k_1B_1c_1\right)V'(\xi) - B_1^2\,V''(\xi) = 0,$$
$$V^3(\xi) + \left(\frac{c_1k_1^2 + w}{c_2}\right)V(\xi) + \frac{2k_1B_1}{c_2}\,V'(\xi) - \frac{B_1^2c_1}{c_2}\,V''(\xi) = 0,$$

respectively. Therefore, by assuming

$$c_1 = c_2, \qquad w = -\gamma c_2, \qquad \nu = -\frac{2k_1B_1(1+c_2^2)}{c_2},$$

we reach to a unique ODE

$$V^3(\xi) + \left(k_1^2 - \gamma\right)V(\xi) + \frac{2k_1B_1}{c_2}\,V'(\xi) - B_1^2\,V''(\xi) = 0. \tag{13}$$

In the rest of paper, we investigate the soliton solutions of the model by using the reduced ODE (13). Moreover, bifurcation, chaotic behavior, and sensitivity analysis will be investigated for the Eq. (13).

3.1 The second degree GAEM

This paper utilizes the variable coefficient second-degree GAEM to obtain exact solutions for the KTE. This innovative technique proposed by Hashemi et al. in [11, 12] extends Abel's equation by incorporating variable coefficients, allowing for the effective resolution of complex nonlinear equations within stochastic quantum mechanics. By broadening the scope of Abel's equation, this approach establishes a robust framework for analyzing

the intricate dynamics of quantum systems influenced by stochastic processes. The flexibility of this methodology highlights its potential for solving a diverse range of nonlinear equations across multiple scientific and engineering fields.

To begin, we outline a method for deriving equations

$$V' = \mathscr{K}_2(\xi)\,V^2 + \mathscr{K}_1(\xi)\,V + \mathscr{K}_0(\xi) \tag{14}$$

from a provided Eq. (13). Let us assume that $V = V(\xi)$ denotes any solution of Eq. (14). Then

$$V''(\xi) = \mathscr{K}_2'\,V^2 + \mathscr{K}_1'\,V + \mathscr{K}_0' + V'[2\mathscr{K}_2\,V + \mathscr{K}_1].$$

Therefore, from Eq. (14) we have

$$\begin{aligned} V''(\xi) = {} & 2\mathscr{K}_2^2\,V^3 + (\mathscr{K}_2' + 3\mathscr{K}_1\mathscr{K}_2)\,V^2 \\ & + \left(\mathscr{K}_1' + \mathscr{K}_1^2 + 2\mathscr{K}_0\mathscr{K}_2\right)V + (\mathscr{K}_0' + \mathscr{K}_0\mathscr{K}_1). \end{aligned}$$

The core concept of this analytical technique is explained as follows: by substituting the recent obtained expressions V', V'' into Eq. (13), one can obtain a polynomial with respect to V. Hence, equating the coefficients of this polynomial to zero yields an overdetermined system of differential-algebraic equations for the functions $\mathscr{K}_i(\xi)$, where $0 \leqslant i \leqslant 2$. If a solution for $\mathscr{K}_0(\xi)$, $\mathscr{K}_1(\xi)$, $\mathscr{K}_2(\xi)$ of this system exists, then any solution to Eq. (14) will also satisfy Eq. (13). Inserting Eq. (14) into Eq. (13) yields in a third-degree polynomial with respect to V in the form

$$\sum_{i=0}^{3} S_i\,V^i = 0,$$

where

$$\begin{aligned} S_0 &= -B_1^2c_2\left(\frac{\mathrm{d}}{\mathrm{d}\xi}\mathscr{K}_0(\xi)\right) - B_1^2c_2\mathscr{K}_1(\xi)\mathscr{K}_0(\xi) + 2B_1k_1\mathscr{K}_0(\xi) \\ S_1 &= -B_1^2c_2\left(\frac{\mathrm{d}}{\mathrm{d}\xi}\mathscr{K}_1(\xi)\right) - B_1^2\mathscr{K}_1(\xi)^2c_2 + 2B_1k_1\mathscr{K}_1(\xi) \\ &\quad - 2B_1^2c_2\mathscr{K}_0(\xi)\mathscr{K}_2(\xi) + c_2(k_1^2 - \gamma), \\ S_2 &= -B_1^2c_2\left(\frac{\mathrm{d}}{\mathrm{d}\xi}\mathscr{K}_2(\xi)\right) - 3B_1^2c_2\mathscr{K}_2(\xi)\mathscr{K}_1(\xi) + 2B_1k_1\mathscr{K}_2(\xi), \\ S_3 &= -2B_1^2\mathscr{K}_2(\xi)^2c_2 + c_2. \end{aligned}$$

By setting $S_i = 0$, $i \in \{0, 1, 2, 3\}$, we get a differential-algebraic system, which leads to the following families of solutions:

Family 1:

$$\mathscr{K}_0(\xi) = 0, \qquad \mathscr{K}_1(\xi) = \frac{2}{B_1}\sqrt{\frac{\gamma}{9c_2^2+8}}, \qquad \mathscr{K}_2(\xi) = \frac{\sqrt{2}}{2B_1}, \qquad k_1 = 3c_2\sqrt{\frac{\gamma}{9c_2^2+8}}.$$

Under these circumstances, Eq. (14) transforms to

$$\frac{\mathrm{d}}{\mathrm{d}\xi}V(\xi) = \frac{V}{2B_1}(\xi)\left[\sqrt{2}\,V(\xi) + 4\sqrt{\frac{\gamma}{9c_2^2+8}}\right]. \tag{15}$$

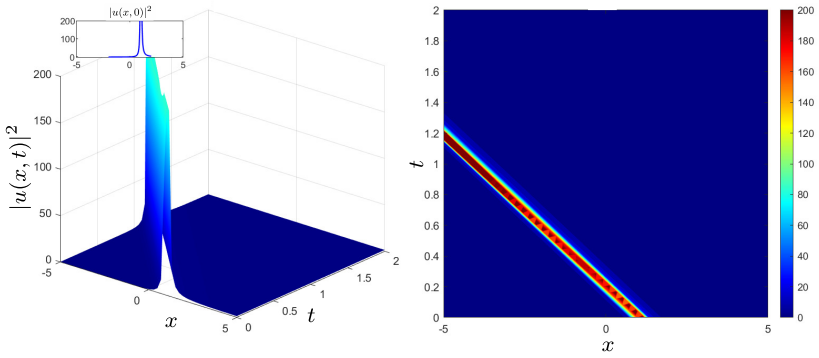


Figure 2. 3D plots and contour plots of $|u(x,t)|^2$ in Eq. (9).

Obviously, an exact solution to Eq. (15) is also a solution to Eq. (13). The exact solution to Eq. (15) can be formulated as

$$V(\xi) = 4\sqrt{\frac{\gamma}{9c_2^2+8}}\left[4\mathrm{e}^{-2\sqrt{\gamma/(9c_2^2+8)}\,\xi/B_1}R_1\sqrt{\frac{\gamma}{9c_2^2+8}} - \sqrt{2}\right]^{-1},$$

where $R_1 \in \mathbb{R}$. Therefore, the final solution can be written in the following form:

$$u(x,t) = -4\gamma\mathrm{e}^{\mathrm{i}(3c_2x\sqrt{\gamma/(9c_2^2+8)}+\gamma c_2 t-\theta)}\left[\sqrt{2}\big[9c_2^2+8\big]\sqrt{\frac{\gamma}{9c_2^2+8}}\right.$$
$$\left. - 4\mathrm{e}^{-12((c_2^2+1)t\sqrt{\gamma/(9c_2^2+8)}+x/6)\sqrt{\gamma/(9c_2^2+8)}}R_1\gamma\right]^{-1}. \tag{16}$$

Figure 2 shows a singular solution of $|u(x,t)|^2$ in Eq. (16) with respect to the parameters $c_2 = 1$, $\theta = -2$, $\gamma = 3$, and $R_1 = 2$.

Family 2:

$$\mathscr{K}_0(\xi) = 0, \qquad \mathscr{K}_1(\xi) = -\frac{2}{B_1}\sqrt{\frac{\gamma}{9c_2^2+8}}, \qquad \mathscr{K}_2(\xi) = \frac{\sqrt{2}}{2B_1}, \qquad k_1 = -3c_2\sqrt{\frac{\gamma}{9c_2^2+8}}.$$

Under these circumstances, Eq. (14) transforms to

$$\frac{\mathrm{d}}{\mathrm{d}\xi}V(\xi) = \frac{V(\xi)}{2B_1}\left[\sqrt{2}\,V(\xi) - 4\sqrt{\frac{\gamma}{9c_2^2+8}}\right]. \tag{17}$$

Obviously, an exact solution to Eq. (17) is also a solution to Eq. (13). Therefore,

$$V(\xi) = 4\sqrt{\frac{\gamma}{9c_2^2+8}}\left[4\mathrm{e}^{2\sqrt{\gamma/(9c_2^2+8)}\,\xi/B_1}R_1\sqrt{\frac{\gamma}{9c_2^2+8}} + \sqrt{2}\right]^{-1},$$

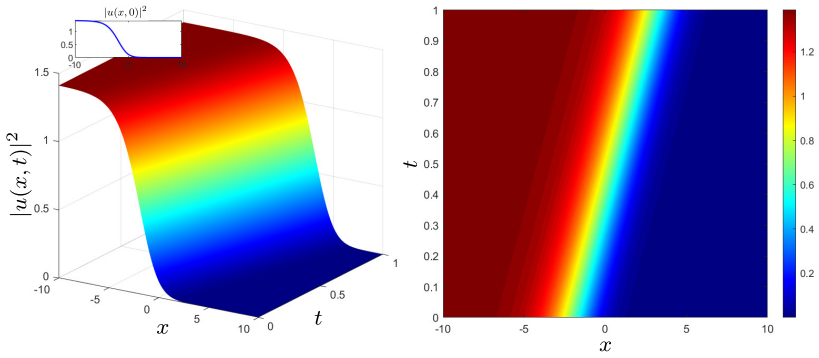


Figure 3. 3D plots and contour plots of $|u(x,t)|^2$ in Eq. (18).

where $R_1 \in \mathbb{R}$. Therefore, one can write the final solution in the following form:

$$u(x,t) = 4\gamma e^{i(3c_2 x\sqrt{\gamma/(9c_2^2+8)} - \gamma c_2 t + \theta)} \Bigg[\sqrt{2}\left(9c_2^2+8\right)\sqrt{\frac{\gamma}{9c_2^2+8}} + 4e^{-12((c_2^2+1)t\sqrt{\gamma/(9c_2^2+8)} - x/6)\sqrt{\gamma/(9c_2^2+8)}} R_1 \gamma\Bigg]^{-1}. \tag{18}$$

Figure 3 shows a kink soliton solution of $|u(x,t)|^2$ in Eq. (18) with respect to the parameters $c_2 = 1$, $\theta = -2$, $\gamma = 3$, and $R_1 = 2$.

4 Bifurcation and dynamical behavior of the KTE

Chaos and bifurcation analysis are crucial in understanding the behavior of complex PDEs, such as the KTE, which models synchronization phenomena in systems with many interacting oscillators. Chaos refers to the sensitive dependence on initial conditions, where small changes can lead to vastly different outcomes, making long-term prediction difficult. Bifurcation analysis explores how the qualitative nature of solutions changes as parameters vary, revealing critical thresholds where new patterns emerge [21, 27].

In the context of the KTE, this analysis helps identify the conditions under which synchronization transitions occur, providing insights into the stability and dynamics of the system. Understanding these phenomena is essential for applications in various fields, including physics, biology, and engineering, where complex interactions give rise to emergent behaviors.

In this section, we will investigate the dynamic properties of the KTE under the influence of the traveling wave transformation described by Eq. (12). Clearly, by assuming $V(\xi) = \Psi(\xi)$, the associated dynamical system of Eq. (13) can be written as

$$\frac{d\Psi}{d\xi} = Y, \qquad \frac{dY}{d\xi} = \widetilde{\mathcal{A}}Y + \widehat{\mathcal{A}}\Psi + \overline{\mathcal{A}}\Psi^3, \tag{19}$$

where

$$\widetilde{\mathcal{A}} = \frac{2k_1}{c_2 B_1}, \qquad \widehat{\mathcal{A}} = \frac{k_1^2 - \gamma}{B_1^2}, \qquad \overline{\mathcal{A}} = \frac{1}{B_1^2}.$$

4.1 Bifurcation and phase portraits

Bifurcation analysis is the study of how the qualitative structure of a dynamical system's phase portrait changes as one or more parameters are varied [3, 16, 21, 26]. At its core, this analysis identifies critical parameter values—called bifurcation points—where the system's equilibrium points, limit cycles, or other invariant sets undergo topological changes, such as birth, death, or stability shifts. The phase portrait, which visually maps the system's trajectories in state space, serves as the central tool for this investigation; by examining how these portraits evolve with the parameter, one can classify bifurcations into canonical types like saddle-node, Hopf, or pitchfork. Together, bifurcation analysis and phase portraits provide a powerful framework for understanding not only the stability and long-term behavior of a system but also the critical thresholds at which its dynamics fundamentally reorganize.

According to the dynamical system (19), we assume $\Xi(Y,\Psi) = Y$ and $\Lambda(Y,\Psi) = \widetilde{\mathcal{A}}Y + \widehat{\mathcal{A}}\Psi + \overline{\mathcal{A}}\Psi^3$. Then solving $\Xi(Y,\Psi) = \Lambda(Y,\Psi) = 0$ yields the equilibrium points (Y_e, Ψ_e) of the considered model as follows:

$$\mathscr{P}_0 = (0,0), \qquad \mathscr{P}_1 = \big(\sqrt{\gamma - k_1^2},\, 0\big), \qquad \mathscr{P}_2 = \big(-\sqrt{\gamma - k_1^2},\, 0\big).$$

Equilibrium points can be classified into various types based on their stability and behavior, such as the saddle point, center point, node point, and cusp point. In order to distinguish various types of equilibrium points, we need the following relations.

For the considered system (19), the Jacobian matrix can be represented as

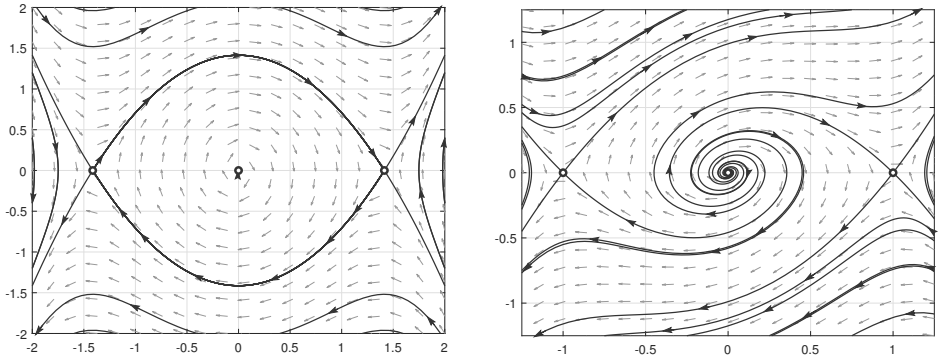
$$\mathscr{J}(Y_e,\Psi_e) = \begin{bmatrix} \frac{\mathrm{d}\Xi(Y,\Psi)}{\mathrm{d}\Psi} & \frac{\mathrm{d}\Xi(Y,\Psi)}{\mathrm{d}Y} \\ \frac{\mathrm{d}\Lambda(Y,\Psi)}{\mathrm{d}\Psi} & \frac{\mathrm{d}\Lambda(Y,\Psi)}{\mathrm{d}Y} \end{bmatrix} = \begin{bmatrix} 0 & 1 \\ 3\overline{\mathcal{A}}\Psi^2 + \widehat{\mathcal{A}} & \widetilde{\mathcal{A}} \end{bmatrix}.$$

Moreover, for the obtained Jacobian, we define

$$\begin{aligned} \mathscr{D}_0 &= \det\big(\mathscr{J}(Y_e,\Psi_e)\big) = -3\overline{\mathcal{A}}\Psi^2 - \widehat{\mathcal{A}}, \\ \mathscr{D}_1 &= \operatorname{trace}\big(\mathscr{J}(Y_e,\Psi_e)\big) = \widetilde{\mathcal{A}}, \\ \mathscr{D}_2 &= \big(\operatorname{trace}\big(\mathscr{J}(Y_e,\Psi_e)\big)\big)^2 = \widetilde{\mathcal{A}}^2. \end{aligned}$$

Lemma 1. (*See* [19, 26].) *For the considered dynamical system* (19)*, we have*:

- *If* $\mathscr{D}_0 > 0$ *and* $\mathscr{D}_1 = 0$*, then* (Y_e, Ψ_e) *is a center point*;
- *If* $\mathscr{D}_0 < 0$*, then* (Y_e, Ψ_e) *is a saddle point*;
- *If* $\mathscr{D}_0 > 0$ *and* $\mathscr{D}_2 - 4\mathscr{D}_0 > 0$*, then* (Y_e, Ψ_e) *is a node point*;
- *If* $\mathscr{D}_0 > 0$*,* $\mathscr{D}_2 - 4\mathscr{D}_0 < 0$*, and* $\mathscr{D}_1 \neq 0$*, then* (Y_e, Ψ_e) *is a focus point.*



(a) $\mathscr{P}_0$-center and $\mathscr{P}_1$, $\mathscr{P}_2$-saddle points (b) $\mathscr{P}_0$-saddle and $\mathscr{P}_1$, $\mathscr{P}_2$-center points

Figure 4. Phase portraits of dynamical system (19).

Now, according to Lemma 1, for the equilibrium points $\mathscr{P}_i$, $i = 1, 2, 3$, we calculate the following necessary values:

$$\mathscr{D}_0\big|_{\mathscr{P}_0} = -\widehat{\mathcal{A}} = \frac{\gamma - k_1^2}{B_1^2}, \qquad \mathscr{D}_0\big|_{\mathscr{P}_1} = \mathscr{D}_0\big|_{\mathscr{P}_2} = 2\widehat{\mathcal{A}} = \frac{2(k_1^2 - \gamma)}{B_1^2},$$

$$\mathscr{D}_1\big|_{\mathscr{P}_0} = \mathscr{D}_1\big|_{\mathscr{P}_1} = \mathscr{D}_1\big|_{\mathscr{P}_2} = \widetilde{\mathcal{A}} = \frac{2k_1}{c_2 B_1},$$

$$\mathscr{D}_2 - 4\mathscr{D}_0\big|_{\mathscr{P}_0} = \frac{4}{c_2^2 B_1^2}\big[k_1^2 + c_2^2\big(k_1^2 - \gamma\big)\big],$$

$$\mathscr{D}_2 - 4\mathscr{D}_0\big|_{\mathscr{P}_1} = \mathscr{D}_2 - 4\mathscr{D}_0|_{\mathscr{P}_2} = \frac{4}{c_2^2 B_1^2}\big[k_1^2 - 2c_2^2\big(k_1^2 - \gamma\big)\big].$$

Let us investigate the phase portrait with certain parameter values:

(i) With the parameters $a = 2$, $k_1 = 0$, and $B_1 = c_2 = 1$, we have

$$\mathscr{D}_0|_{\mathscr{P}_0} = 2 > 0, \qquad \mathscr{D}_1|_{\mathscr{P}_0} = 0, \qquad \mathscr{D}_2 - 4\mathscr{D}_0|_{\mathscr{P}_0} = -8 < 0$$

and

$$\mathscr{J}_0|_{\mathscr{P}_1} = \mathscr{D}_0|_{\mathscr{P}_2} = -4 < 0, \qquad \mathscr{D}_2 - 4\mathscr{D}_0|_{\mathscr{P}_1} = \mathscr{D}_2 - 4\mathscr{D}_0|_{\mathscr{P}_2} = 16 > 0.$$

Therefore, $\mathscr{P}_0 = (0, 0)$ is a center point, and $\mathscr{P}_1 = (\sqrt{2}, 0)$, $\mathscr{P}_2 = (-\sqrt{2}, 0)$ are saddle points. The corresponding phase portrait is illustrated in Fig. 4(a).

(ii) For $k_1 = B_1 = 1$, $\gamma = 2$, and $c_1 = 5$, we have

$$\mathscr{D}_0|_{\mathscr{P}_0} = 1 > 0, \qquad \mathscr{D}_1|_{\mathscr{P}_0} = 0.4, \qquad \mathscr{D}_2 - 4\mathscr{D}_0|_{\mathcal{E}_0} = -3.84 < 0.$$

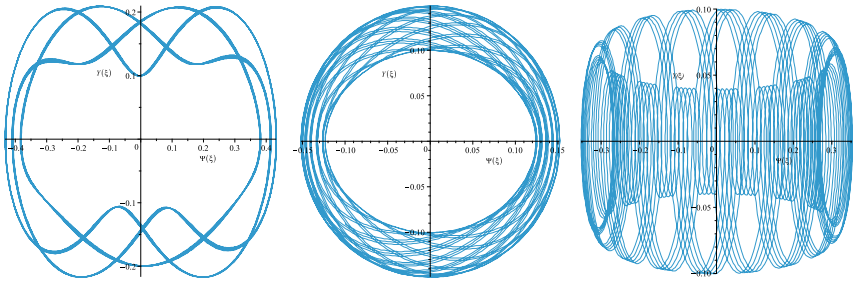
Therefore, $\mathscr{P}_0 = (0, 0)$ is a focus point, and from $\mathscr{D}_0|_{\mathscr{P}_1} = \mathscr{D}_0|_{\mathscr{P}_2} = -2 < 0$ we have the saddle points $\mathscr{P}_1 = (1, 0)$, $\mathscr{P}_2 = (-1, 0)$. Corresponding phase portrait is plotted in Fig. 4(b).

4.2 Chaotic behavior

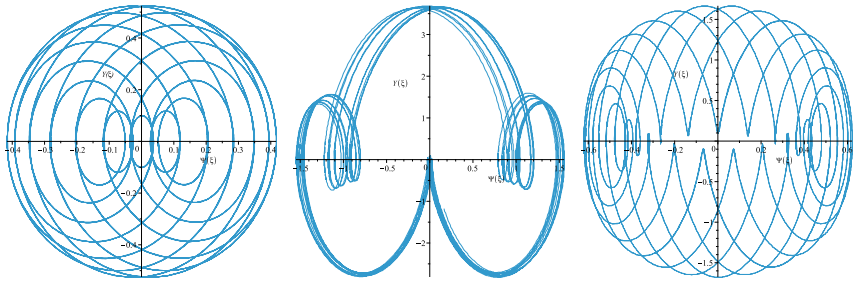
The chaotic behavior of a dynamical system, particularly one derived from the KTE (5), is characterized by sensitive dependence on initial conditions and complex, unpredictable patterns. The KTE models the synchronization of oscillators, where the interplay between coupling strength and natural frequencies can lead to a rich variety of dynamical behaviors, including periodic, quasi-periodic, and chaotic regimes. In chaotic states, small variations in the initial parameters can result in vastly different trajectories, making long-term prediction impossible. This chaotic dynamics is often visualized through bifurcation diagrams and phase portraits, revealing intricate structures that highlight the system's underlying complexity and the transition between order and chaos [14, 20]. We explore the dynamics of the previously mentioned system in our analysis:

$$\frac{\mathrm{d}\Psi}{\mathrm{d}\xi} = Y, \qquad \frac{\mathrm{d}Y}{\mathrm{d}\xi} = \widetilde{\mathcal{A}}Y + \widehat{\mathcal{A}}\Psi + \overline{\mathcal{A}}\Psi^3 + \varkappa_1 \sin(\varkappa_2 \xi). \tag{20}$$

To perform a full numerical simulation of the phase diagrams for the considered system, the parameters are assigned as $k_1 = 0$, $\gamma = 2$, and $B_1 = c_2 = 1$. As shown in Figs. 5(a)–5(f), the perturbed system defined by system (20) displays chaotic behavior. Furthermore, changes in the amplitude $\varkappa_1$ and frequency $\varkappa_2$ lead to distinct chaotic features. Moreover,

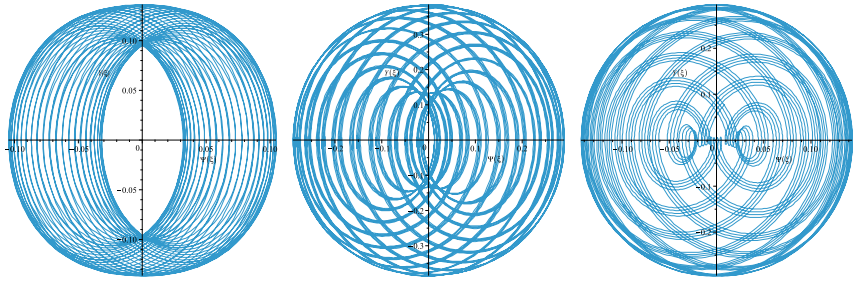


(a) $\varkappa_1 = 1$, $\varkappa_2 = 0.5$ (b) $\varkappa_1 = 0.3$, $\varkappa_2 = 0.9$ (c) $\varkappa_1 = 0.9$, $\varkappa_2 = 0.1$

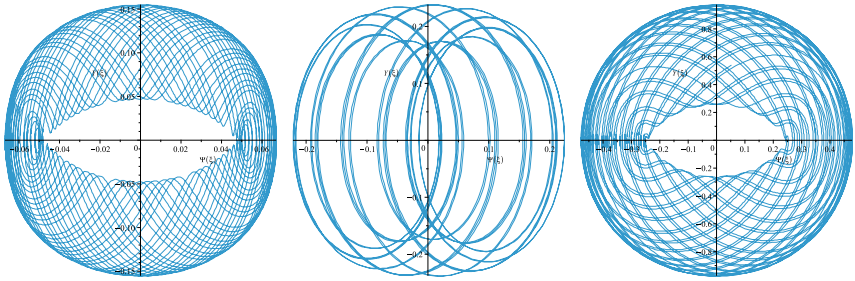


(d) $\varkappa_1 = -0.5$, $\varkappa_2 = 0.9$ (e) $\varkappa_1 = -8$, $\varkappa_2 = 5$ (f) $\varkappa_1 = 6$, $\varkappa_2 = 8$

Figure 5. Chaotic behaviors of system (20) using different $\varkappa_1$ and $\varkappa_2$.



(a) $\varkappa_1 = 0.1$, $\varkappa_2 = 0.5$ (b) $\varkappa_1 = 0.3$, $\varkappa_2 = 0.9$ (c) $\varkappa_1 = 0.2$, $\varkappa_2 = 0.8\pi$



(d) $\varkappa_1 = 0.1\pi$, $\varkappa_2 = 2\pi$ (e) $\varkappa_1 = 0.3$, $\varkappa_2 = 0.1\pi$ (f) $\varkappa_1 = 0.8$, $\varkappa_2 = -\pi$

Figure 6. Chaotic behaviors of system (21) using different $\varkappa_1$ and $\varkappa_2$.

let us explore the dynamics of the system in the following format:

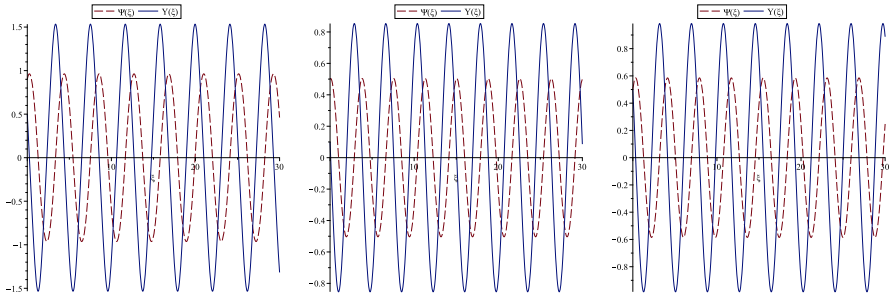
$$\frac{\mathrm{d}\Psi}{\mathrm{d}\xi} = Y, \qquad \frac{\mathrm{d}Y}{\mathrm{d}\xi} = \widetilde{\mathcal{A}}Y + \widehat{\mathcal{A}}\Psi + \overline{\mathcal{A}}\Psi^3 + \varkappa_1 \cos(\varkappa_2 \xi). \tag{21}$$

Similarly to the previous case, by choosing the parameters $k_1 = 0$, $\gamma = 2$, and $B_1 = c_2 = 1$, we plot the chaotic behavior of perturbed system (21) in Figs. 6(a)–6(f).

4.3 Sensitivity analysis

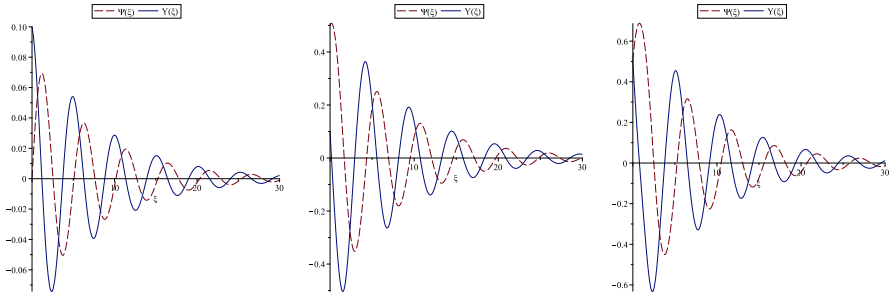
Sensitivity analysis of dynamical systems involves investigating how small changes in system parameters or initial conditions affect the system's behavior over time. It is crucial because it helps identify which parameters have the most significant impact on system dynamics, enabling better model calibration, prediction accuracy, and control design. By understanding sensitivity, researchers and engineers can assess system robustness, optimize performance, and anticipate possible instabilities or unexpected behaviors, making it an essential tool in fields ranging from engineering to biology and economics. Let us investigate the sensitivity analysis of Eqs.(5) with various initial conditions.

Figures 7(a)–7(c) are presented for the parameter values $k_1 = 0$, $\gamma = 3$, and $B_1 = c_2 = 1$. These plots indicate that the system under consideration shows little response to small changes in initial conditions. Figure 7(a) is plotted with respect to the initial



(a) (b) (c)

Figure 7. Sensitive analysis of the dynamical system (19) with respect to $k_1 = 0$, $\gamma = 3$, and $B_1 = c_2 = 1$ for different initial conditions.



(a) (b) (c)

Figure 8. Sensitive analysis of the dynamical system (19) with respect to $k_1 = 0.1$, $\gamma = c_2 = 1$, and $B_1 = -0.8$ for different initial conditions.

conditions $\Psi(0) = 0$, $Y(0) = 0.1$, whereas the initial conditions for Fig. 7(b) are $\Psi(0) = 0.5$, $Y(0) = 0.1$, and those for Fig. 7(c) are $\Psi(0) = 0.5$, $Y(0) = 0.5$.

Figures 8(a)–8(c) are plotted with respect to the parameters values $k_1 = 0.1$, $\gamma = c_2 = 1$, and $B_1 = -0.8$. These plots indicate that the system under consideration shows small response to small changes in initial conditions. Figure 8(a) is plotted with respect to the initial conditions $\Psi(0) = 0$, $Y(0) = 0.1$, whereas the initial conditions for Fig. 8(b) are $\Psi(0) = 0.5$, $Y(0) = 0.1$, and those for Fig. 8(c) are $\Psi(0) = 0.5$, $Y(0) = 0.5$.

5 Conclusion

In conclusion, this paper presents a comprehensive analysis of the KTE model, focusing on its exact solutions, Lie symmetries, and dynamical behavior. We successfully derived soliton solutions, highlighting the model's intricate dynamics. These solutions—including dark solitons and singular solutions—capture the underlying physical behavior of the system, offering insight into how the governing parameters shape the qualitative behavior of the solutions. The application of the Nucci reduction technique facilitated the

derivation of several invariant solutions, demonstrating its utility in simplifying complex equations. Additionally, we utilized the second-degree GAEM recently introduced by Hashemi et al. to obtain further soliton solutions, showcasing the effectiveness of this innovative approach. A comparison of the solution families obtained through these two methods confirms their consistency, while also illustrating the complementary strengths each technique offers for tackling nonlinear evolution equations of this type. In addition, we consider the bifurcation, chaotic behavior, and sensitivity analysis of the dynamical system associated with the KTE, revealing the rich and complex nature of its dynamics. The presence of chaotic regimes under specific parameter regimes underscores the sensitivity of the system to initial conditions and parameter perturbations, which carries important implications for the predictability and control of the underlying physical process. Overall, our findings contribute to a deeper understanding of synchronization phenomena and the mathematical techniques applicable to nonlinear systems, paving the way for future research in this area. For the follow-up studies to be conducted next, first, the current analysis of the KTE model completed in this paper can be extended to several derivative versions of this model, that is, higher-dimensional versions, fractional-order versions, or versions with added stochastic characteristics. In addition to extending the existing analysis to new model variants, future research must also supplement two types of verification for the model solutions calculated in this paper: one is verification completed through numerical computation, and the other is verification carried out through practical experiments, to confirm that the obtained solutions are valid. Beyond that, future research can also explore more available new methods, including one category of new methods for pure theoretical analysis, and another category of methods assisted by machine learning, to fully excavate the rich characteristics in the dynamic changes of this model through these methods. The aforementioned research extensions can also pave the way for applying the entire framework of the KTE model to practical scenarios. Among these practical scenarios that can adopt this framework, synchronization phenomena and nonlinear wave phenomena are exactly the core influencing factors.

Author contributions. All authors (M.S.H., M.K.A., M.E.S., K.H., and M.B.) contributed equally to this work. All authors have read and approved the published version of the manuscript.

Conflicts of interest. The authors declare no conflicts of interest.

References

1. I.S. Aranson, L. Kramer, The world of the complex Ginzburg-Landau equation, *Rev. Mod. Phys.*, **74**(1):99, 2002, https://doi.org/10.1103/RevModPhys.74.99.

2. Y. Chahlaoui, A.R. Butt, H. Abbas, A. Bekir, Novel exact traveling wave solutions of Newton-Schrödinger system using Nucci reduction and Sardar sub-equation methods, *Phys. Scr.*, **99**(8): 085227, 2024, https://doi.org/10.1088/1402-4896/ad604c.

3. Y. Chen, Z.-W. Liu, Y. Qin, Finite-time topology identification of delayed complex dynamical networks and its application, *Cyborg Bionic Syst.*, **5**:0092, 2024, https://doi.org/10.34133/cbsystems.0092.
4. M. Cinar, A. Secer, M.S. Hashemi, M. Ozisik, M. Bayram, A comprehensive analysis of Fokas–Lenells equation using Lie symmetry method, *Math. Methods Appl. Sci.*, **47**(7):5819–5830, 2024, https://doi.org/10.1002/mma.9892.
5. S. Dong, X. Zhang, Y. Jin, A second order convergent difference scheme for the initial-boundary value problem of Rosenau-Burgers equation, *Electron. J. Differ. Equ.*, **2024**:38, 2024, https://doi.org/10.58997/ejde.2024.38.
6. X. Dong, A fourth-order split-step pseudospectral scheme for the Kuramoto–Tsuzuki equation, *Commun. Nonlinear Sci. Numer. Simul.*, **17**(8):3161–3168, 2012, https://doi.org/10.1016/j.cnsns.2011.12.020.
7. M. Elbrolosy, A. Elmandouh, Painlevé analysis, Lie symmetry and bifurcation for the dynamical model of radial dislocations in microtubules, *Nonlinear Dyn.*, **113**:13699–13714, 2025, https://doi.org/10.1007/s11071-025-11084-5.
8. M. Eslami, H. Rezazadeh, The first integral method for Wu–Zhang system with conformable time-fractional derivative, *Calcolo*, **53**(3):475–485, 2016, https://doi.org/10.1007/s10092-015-0158-8.
9. V. García-Morales, K. Krischer, The complex Ginzburg–Landau equation: an introduction, *Contemp. Phys.*, **53**(2):79–95, 2012, https://doi.org/10.1080/00107514.2011.642554.
10. T. Guo, Q. Shi, Vanishing diffusion limits for a mixed-dissipation complex Ginzburg-Landau equation, *Discrete Contin. Dyn. Syst., Ser. S*, 2026, https://doi.org/10.3934/dcdss.2026205.
11. M.S. Hashemi, A variable coefficient third degree generalized Abel equation method for solving stochastic Schrödinger–Hirota model, *Chaos Solitons Fractals*, **180**:114606, 2024, https://doi.org/10.1016/j.chaos.2024.114606.
12. M.S. Hashemi, M. Bayram, M.B. Riaz, D. Baleanu, Bifurcation analysis, and exact solutions of the two-mode Cahn–Allen equation by a novel variable coefficient auxiliary equation method, *Results Phys.*, **64**:107882, 2024, https://doi.org/10.1016/j.rinp.2024.107882.
13. F Ivanauskas, On convergence of difference schemes for nonlinear Schrödinger equations, the Kuramoto-Tsuzuki equation, and reaction-diffusion type systems, *Lith. Math. J.*, **34**(1):30–44, 1994, https://doi.org/10.1007/BF02335388.
14. J. Jin, W. Chen, A. Ouyang, F. Yu, H. Liu, A time-varying fuzzy parameter zeroing neural network for the synchronization of chaotic systems, *IEEE Trans. Emerging Top. Comput. Intell.*, **8**(1):364–376, 2024, https://doi.org/10.1109/TETCI.2023.3301793.
15. S. Kumar, S.K. Dhiman, Exploring cone-shaped solitons, breather, and lump-forms solutions using the Lie symmetry method and unified approach to a coupled breaking soliton model, *Phys. Scr.*, **99**(2):025243, 2024, https://doi.org/10.1088/1402-4896/ad1d9e.
16. S. Kumar, S. Rani, N. Mann, Analytical soliton solutions to a $(2+1)$-dimensional variable coefficients graphene sheets equation using the application of Lie symmetry approach: Bifurcation theory, sensitivity analysis and chaotic behavior, *Qual. Theory Dyn. Syst.*, **24**(2):80, 2025, https://doi.org/10.1007/s12346-025-01232-y.

17. Y. Kuramoto, T. Tsuzuki, On the formation of dissipative structures in reaction-diffusion systems: Reductive perturbation approach, *Prog. Theor. Phys.*, **54**(3):687–699, 1975, https://doi.org/10.1143/PTP.54.687.
18. S. Labidi, K. Omrani, A new approach for numerical solution of Kuramoto-Tsuzuki equation, *Appl. Numer. Math.*, **184**:527–541, 2023, https://doi.org/10.1016/j.apnum.2022.11.004.
19. J. Li, G. Chen, Bifurcations of traveling wave solutions for four classes of nonlinear wave equations, *Int. J. Bifurcation Chaos*, **15**(12):3973–3998, 2005, https://doi.org/10.1142/S0218127405014416.
20. X. Liu, L. Zhao, J. Jin, A noise-tolerant fuzzy-type zeroing neural network for robust synchronization of chaotic systems, *Concurrency Comput. Pract. Exp.*, **36**(22):e8218, 2024, https://doi.org/10.1002/cpe.8218.
21. S. Malik, A. Akbulut, U. Demirbilek, H. Rezazadeh, S. Salahshour, Nonlinear dynamics and bifurcation analysis of integrable models for long wave propagation in plasma physics and oceanography, *Nonlinear Dyn.*, **114**:442, 2026, https://doi.org/10.1007/s11071-025-12154-4.
22. M.C. Nucci, P.G.L. Leach, The determination of nonlocal symmetries by the technique of reduction of order, *J. Math. Anal. Appl.*, **251**(2):871–884, 2000, https://doi.org/10.1006/jmaa.2000.7141.
23. M.C. Nucci, P.G.L. Leach, Jacobi's last multiplier and the complete symmetry group of the Ermakov-Pinney equation, *J. Nonlinear Math. Phys.*, **12**(2):305–320, 2005, https://doi.org/10.2991/jnmp.2005.12.2.10.
24. H. Rezazadeh, New solitons solutions of the complex Ginzburg-Landau equation with Kerr law nonlinearity, *Optik*, **167**:218–227, 2018, https://doi.org/10.1016/j.ijleo.2018.04.026.
25. H. Rezazadeh, M. Inc, D. Baleanu, New solitary wave solutions for variants of (3+1)-dimensional Wazwaz-Benjamin-Bona-Mahony equations, *Front. Phys.*, **8**:332, 2020, https://doi.org/10.3389/fphy.2020.00332.
26. Y. Wang, W.R. Shan, X. Zhou, P.P. Wang, Exact solutions and bifurcation for the resonant nonlinear Schrödinger equation with competing weakly nonlocal nonlinearity and fractional temporal evolution, *Waves Random Complex Media*, **31**(6):1859–1878, 2021, https://doi.org/10.1080/17455030.2019.1706013.
27. R. Wu, W. Xiong, Bifurcation in a Leslie–Gower system with fear in predators and strong Allee effect in prey, *Nonlinear Anal. Model. Control*, **30**(5):793–810, 2025, https://doi.org/10.15388/namc.2025.30.38982.
28. H. Yang, Unconditionally optimal error estimate of the Crank–Nicolson extrapolation Galerkin finite element method for Kuramoto–Tsuzuki equation, *Comput. Appl. Math.*, **42**(6):259, 2023, https://doi.org/10.1007/s40314-023-02397-5.
29. H. Yépez-Martínez, M.S. Hashemi, A.S. Alshomrani, M. Inc, Analytical solutions for nonlinear systems using Nucci's reduction approach and generalized projective Riccati equations, *AIMS Math.*, **8**(7):16655–16690, 2023, https://doi.org/10.3934/math.2023852.
30. Q. Zhang, L. Zhang, Linearly compact difference scheme for the two-dimensional Kuramoto-Tsuzuki equation with the Neumann boundary condition, *Ann. Appl. Math.*, **39**(1):49–78, 2023, https://doi.org/10.4208/aam.OA-2022-0015.